Rare Metal Materials and Engineering
Volume 51, Issue 11, November 2022
Available online at www.rmme.ac.cn

Science Press

Cite this article as: Wan Diqing, Dong Shaoyun, Wang Houbin, et al. Evaluation of Comprehensive Performance of High Damping and High Strength As-Cast $SiC_p/Mg_{94}Zn_5Y_1$ Composites[J]. Rare Metal Materials and Engineering, 2022, 51(11): 4003-4009.

ARTICLE

Evaluation of Comprehensive Performance of High Damping and High Strength As-Cast $SiC_p/Mg_{94}Zn_5Y_1$ Composites

Wan Diqing, Dong Shaoyun, Wang Houbin, Hu Jiajun, Xue Yandan, Han Guoliang, Kang Jie, Zeng Guanmei, Wang Yu, Tang Hao, Yang Fan

School of Materials Science and Engineering, East China Jiaotong University, Nanchang 330013, China

Abstract: $SiC_p/Mg_{94}Zn_5Y_1$ composites with 0.5wt%~2.0wt% SiC_p were prepared by the casting method. The mechanical properties and damping capacities of the composites were investigated. The microstructure and phase components of the composites were analyzed via the scanning electron microscopy and X-ray diffraction. Results show that after the addition of SiC_p into the matrix, the SiC_p is evenly distributed in the matrix, which refines the microstructure of the composite. The $SiC_p/Mg_{94}Zn_5Y_1$ composites contain the α-Mg, I-phase (quasicrystal phase), and SiC_p phase. The damping capacities and mechanical properties of the $SiC_p/Mg_{94}Zn_5Y_1$ composites were evaluated by the dynamic mechanical analyzer and an AG-X testing machine, respectively. The mechanical properties of the composites are better than those of the original $Mg_{94}Zn_5Y_1$ alloy. The 1.0wt% $SiC_p/Mg_{94}Zn_5Y_1$ composite exhibits the compressive strength of 350 MPa. The damping properties of all the composites are much higher than those of the parent alloy. The optimal damping capacity is achieved when the composite contains 0.5wt% SiC_p. Moreover, according to the efficiency coefficient method, the 1.0wt% $SiC_p/Mg_{94}Zn_5Y_1$ composite has the optimal comprehensive properties.

Key words: $SiC_p/Mg_{94}Zn_5Y_1$ composites; quasicrystal; mechanical properties; damping capacities

Magnesium and its alloys have received considerable attention as the promising novel engineering materials due to their high specific strength, low density, and high damping capacities[1-4]. However, the engineering applications of high damping magnesium alloys are restricted due to the discord between their damping and mechanical properties[5]. Adding suitable reinforcement phases into the Mg-based materials can improve the strength and maintain the high damping capacity. Because Mg-based composites also have the advantage of low density, the shorcoming of low stiffness can be overcome. Thus, the Mg-based composites can be used as lightweight nonferrous materials[6-8]. Zhang et al[9] prepared MgO/ZK60 nanocomposites by traditional powder metallurgy, and the composite strength was improved. Yu et al[10] prepared the AZ91D composites reinforced by Ti_2AlC phase with good damping performance. Normally, the mechanical or damping properties of Mg matrix composites can be solely improved. Therefore, the novel Mg matrix composites with both good mechanical and damping properties are required.

The performance of Mg-based composites mainly depends on the matrix, reinforcement, and the bonding strength between the reinforcement and the matrix[11]. The reinforcement phase should have solid load-bearing capacity, good wettability, thermodynamic stability, high hardness, and high elastic modulus[12]. SiC particles (SiC_p) have the advantages of high strength, large modulus, good thermal conductivity, and good wettability with Mg alloy melt[13]. Prasad et al[14] reported that SiC_p can refine the grains and provide good damping properties for the composites. According to Ref. [15], the damping capacity of SiC_p/AZ61 composites is better than that of AZ61 alloy due to the SiC_p addition.

Received date: December 20, 2021
Foundation item: National Natural Science Foundation of China (51665012); Jiangxi Province Science Foundation for Outstanding Scholarship (20171BCB23061, 2018ACB21020); Primary Research & Development Plan of Jiangxi Province (2019BBEL50019)
Corresponding author: Wan Diqing, Ph. D., Professor, School of Materials Science and Technology, East China Jiaotong University, Nanchang 330013, P. R. China, Tel: 0086-791-87046102, E-mail: divadwan@163.com

The Mg-Zn-Y alloys with quasi-crystalline particles are potential high-strength magnesium alloys[16-20], because their quasicrystal phase can improve the mechanical properties of the alloys. However, the damping capacity of the alloy is correspondingly reduced due to the formation of quasicrystal[21]. The synergistic effect of SiC_p and quasicrystal phase (I-phase) in the composites can achieve the favorable coordination between the mechanical and damping properties. However, the properties of coexisting SiC_p and quasicrystal phases in the as-cast Mg-based composites are rarely reported. In this research, the SiC_p ceramic reinforcement phase was added into the Mg-Zn-Y matrix. The mechanical and damping properties of Mg-Zn-Y composites with SiC_p and quasicrystal reinforcement phases were studied, and the strengthening and damping mechanisms were also investigated. Additionally, the mathematical models were used to evaluate the comprehensive properties of the materials.

1 Experiment

The raw Mg ingot (99.9% purity), Zn ingot (99.9% purity), and Mg-Y master alloy (25wt% Y) were used to prepare the $Mg_{94}Zn_5Y_1$ matrix. The SiC_p was selected as the reinforcement phase. Firstly, the pure Mg was placed into a crucible preheated to 300 °C and smelted in a resistance furnace at 720 °C. Once the Mg ingot was completely molten, the Mg-Y master alloy and pure Zn ingot were sequentially added to obtain $Mg_{94}Zn_5Y_1$ alloy. Finally, the 0wt%, 0.5wt%, 1.0wt%, and 2.0wt% SiC_p was separately added into the mixed melt. After stirring at 700 r/min for 90 s in Ar atmosphere, the melt was poured into a steel mold. The composites of different SiC_p contents were produced.

The specimen microstructure was observed by the scanning electron microscope (SEM, Hitachi SU-8010) equipped with energy dispersive spectroscope (EDS). The phase constituent analysis was performed via X-ray diffraction (XRD, Shimadzu XRD-6100) with monochromatic Cu Kα radiation. In addition, the specimens were compressed at 0.5 $mm \cdot min^{-1}$ by the AG-X testing machine (Shimadzu corporation). The damping capacities of specimens were measured by the dynamic mechanical analyzer (DMA Q800, TA Instruments). The strain ranged from 1×10^{-4} to 4×10^{-3} under the conditions of room temperature and frequency of 1 Hz.

2 Results and Discussion

2.1 Microstructure

The microstructures of the as-cast $Mg_{94}Zn_5Y_1$ alloy and different $SiC_p/Mg_{94}Zn_5Y_1$ composites are shown in Fig. 1. It can be seen that the $Mg_{94}Zn_5Y_1$ alloy is composed of the matrix (α-Mg) and a lamellar eutectic phase (α-Mg+I-phase). During the solidification of $Mg_{94}Zn_5Y_1$ alloy, the primary α-Mg phase is firstly crystallized, and the eutectic structure (α-Mg+I-phase) is formed via the pseudo-eutectic reaction[22,23]. Yi et al[23] indicated that the two-phase (α-Mg+I-phase) field exists in the Mg-Zn-Y ternary alloy system when the content ratio of Zn to Y is close to 5 or 6. Kim et al[24] revealed that the α-Mg is firstly crystallized from the melt to form a dendritic morphology, and the remaining liquid in the interdendritic region is solidified into the eutectic structure (α-Mg+I-phase) when the composition changes. Fig. 1b shows the magnificent microstructure of I-phase, namely quasicrystal phase, in the $Mg_{94}Zn_5Y_1$ composite. The eutectic phase can hinder the diffusion of Mg, Zn, and Y elements more effectively than the grainy I-phase does. Therefore, the eutectic phase can refine the α-Mg dendrites more effectively[25]. The SiC_p addition affects the temperature distribution and solute distribution of the solid-liquid, thereby influencing the morphology and growth kinetics of the lamellar eutectic phase. After the SiC_p is added into the matrix (Fig. 1c~1e), the composites are composed of α-Mg dendrites, eutectic phase, and scattered particles. Fig. 2b shows EDS Si element distribution in the

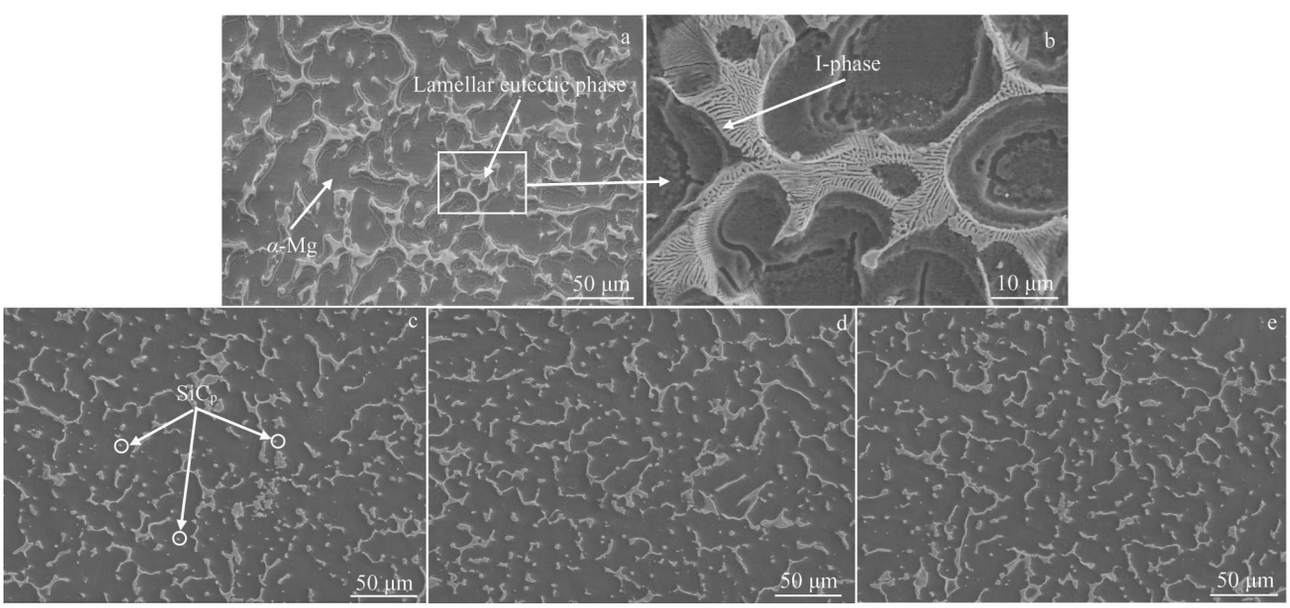

Fig.1 Microstructures of $SiC_p/Mg_{94}Zn_5Y_1$ composites with different SiC_p contents: (a, b) 0wt%, (c) 0.5wt%, (d) 1.0wt%, and (e) 2.0wt%

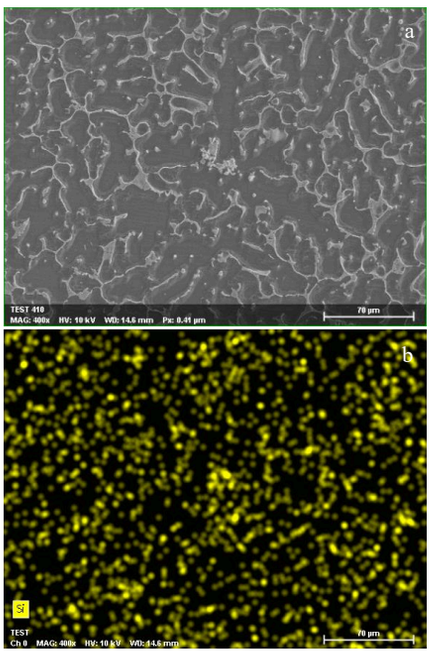

Fig.2 SEM microstructure (a) and corresponding EDS Si element distribution (b) of 0.5wt% $SiC_p/Mg_{94}Zn_5Y_1$ composite

0.5wt% $SiC_p/Mg_{94}Zn_5Y_1$ composite. It can be seen that the Si element is relatively evenly distributed in the matrix. Fig. 3 shows XRD patterns of different $SiC_p/Mg_{94}Zn_5Y_1$ composites. The diffraction peaks are mainly related to the α-Mg, I-phase, and SiC_p phase. According to Fig.2 and Fig.3, the SiC_p stably exists in the matrix and has a phase strengthening effect.

2.2 Compressive properties

The elastic modulus of SiC_p and Mg-based matrix is different. During the compressive deformation process, the SiC_p and Mg-based matrix are coordinatively deformed, i.e., the load is transferred from the soft Mg-based matrix to the hard SiC_p reinforcement phase, which improves the mechanical properties of the composites. Particularly, the I-phase improves the mechanical properties of the composites. Fig.4 shows the compressive stress-strain curves of different $SiC_p/Mg_{94}Zn_5Y_1$ composites. After the SiC_p is added into the matrix, the compressive properties of the $SiC_p/Mg_{94}Zn_5Y_1$ composites are significantly better than those of the $Mg_{94}Zn_5Y_1$ alloy. According to Table 1, the optimal mechanical properties (compressive strength of 350 MPa) are achieved when the SiC_p content is 1.0wt%, which is 12.5% higher than the compressive strength of the $Mg_{94}Zn_5Y_1$ base alloy. With increasing the SiC_p content, the compressive properties of composites are increased firstly and then decreased. When the SiC_p content is 0.5wt% and 1.0wt%, the SiC_p is evenly distributed in the matrix without apparent agglomeration. With further increasing the SiC_p content, the secondary phase strengthening, dislocation strengthening, and other strengthening mechanisms are more obvious. However, when 2wt% SiC_p is added into the matrix, a small amount of SiC_p is agglomerated in the composite and the fine grain strengthening effect is weakened. Thus, the mechanical properties of the material are reduced.

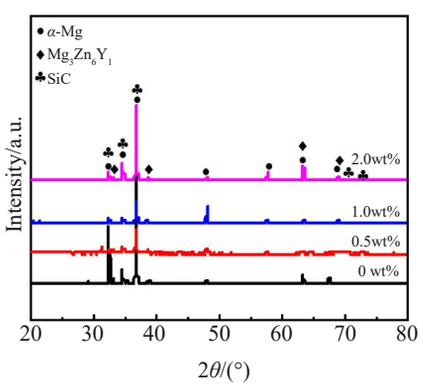

Fig.3 XRD patterns of different $SiC_p/Mg_{94}Zn_5Y_1$ composites

The strengthening mechanism of $SiC_p/Mg_{94}Zn_5Y_1$ composites is primarily related to the secondary phase strengthening, fine grain strengthening, and dislocation strengthening mechanisms. In the SiC_p-reinforced Mg-Zn-Y composites, the thermal expansion coefficient of SiC_p is much smaller than that of the Mg-Zn-Y alloy[26,27], which causes the residual stress in the material. As a result, the plastic deformation occurs in the Mg-based composites, forming the high-density dislocations, and thereby causing the new dislocation strengthening. Furthermore, the α-Mg interdendritic microstructure in the lamellar eutectic phases (α-Mg+I-phase) causes the eutectic phase strengthening effect[28]. The addition of SiC_p has a significant effect on the grain refinement of the matrix alloy. Because the grains are refined, the applied force is increased to activate the sources of dislocations in adjacent grains. A greater external force is required when the fine grains produce the plastic deformation[29].

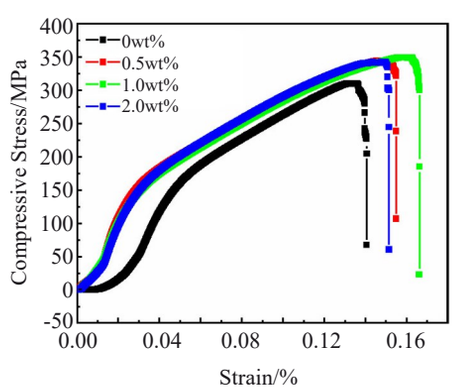

Fig.4 Compressive stress-strain curves of different $SiC_p/Mg_{94}Zn_5Y_1$ composites

Table 1 Mechanical properties of different $SiC_p/Mg_{94}Zn_5Y_1$ composites

SiC_p content/wt%	0	0.5	1.0	2.0
Compressive strength/MPa	311	344	350	342
Compression ratio/%	0.110	0.155	0.166	0.152

2.3 Damping capacities

The damping capacities of the $SiC_p/Mg_{94}Zn_5Y_1$ composites are shown in Fig. 5. It can be seen that all the damping properties of the composites with SiC_p addition are higher than those without the SiC_p addition. The curves can be divided into the strain-amplitude-independent part and the strain-amplitude-dependent part. In the strain-amplitude-independent part, the damping value of the composite is close to that of the matrix alloy. At high strain amplitudes, the damping performance is firstly increased and then decreased with increasing the SiC_p content. Furthermore, after SiC_p is added to the matrix, the critical strain amplitude of all the composites materials is higher than that of the matrix alloy, which indicates that the SiC_p addition improves the damping performance of the matrix alloy. In the strain-amplitude-dependent part, the optimal damping capacity is achieved when the SiC_p content is 0.5wt%. When the SiC_p content is 1.0wt%, different damping mechanisms are functioning well, and the damping value of the 1.0wt% $SiC_p/Mg_{94}Zn_5Y_1$ composite is close to that of the 0.5wt% $SiC_p/Mg_{94}Zn_5Y_1$ composite. The damping value Q_d^{-1} of the $SiC_p/Mg_{94}Zn_5Y_1$ composites at the strain of 4×10^{-4} is shown in Fig. 5b. It is known that when the damping capacity of the material is over 0.01, the material is a high damping material[21]. It can be seen that the damping value of all the composites with SiC_p addition is greater than 0.01, indicating that the $SiC_p/Mg_{94}Zn_5Y_1$ composites are the high-damping materials. In addition, the 0.5wt% $SiC_p/Mg_{94}Zn_5Y_1$ composite shows the highest damping value of 0.011 80.

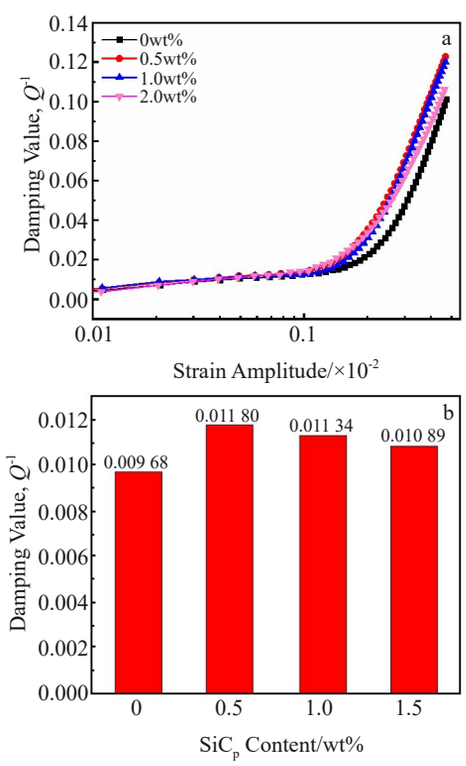

Fig.5 Damping value Q^{-1}-strain amplitude curves (a) and damping value Q^{-1} at strain of 4×10^{-4} (b) of different $SiC_p/Mg_{94}Zn_5Y_1$ composites

Generally, the damping mechanism of Mg-based alloys is related to the dislocations and dominated by the Granato-Lücke (G-L) theory[30,31], which proves that the dislocations are pinned by strong pinners (dislocation nodes, secondary phases, and grain boundaries) and weak pinners (impurity atoms, vacancies, and disorders). At low strain amplitudes, the dislocations are reciprocating between the weak pinners, and the damping is independent of or weakly dependent on the strain amplitude. With increasing the strain amplitude, the dislocations break away from the weak pinners and slip between the strong pinners. The damping capacity of the composites is increased with increasing the strain amplitude. The dislocation damping (Q_d^{-1}), strain-independent partial damping capacity (Q_0^{-1}), and strain-related partial damping capacity (Q_h^{-1}) can be expressed by Eq.(1~3), respectively, as follows:

$$Q_d^{-1} = Q_0^{-1} + Q_h^{-1} \tag{1}$$

$$Q_0^{-1} = \frac{\rho B L_C^4 \omega}{36 G \boldsymbol{b}^2} \tag{2}$$

$$Q_h^{-1} = \frac{C_1}{\varepsilon}\exp\left(-\frac{C_2}{\varepsilon}\right) \tag{3}$$

$$C_1 = \frac{\rho F_B L_N^3}{6|\boldsymbol{b}|EL_C^2}\ C_2 = \frac{F_B}{|\boldsymbol{b}|EL_C} \tag{4}$$

where ρ is the density of a removable dislocation; B is the damping constant; L_N and L_C are the average distances between successive strong pinners and successive weak pinners, respectively; ω is the angular frequency; F_B is binding force between the weak pinners and the dislocations; $\boldsymbol{b}$ is the Burgers vector; G is the shear modulus; E is the elastic modulus; ε is the strain.

The G-L model considers that the dislocation in the crystal is strongly pinned by the immobile defects, such as grain boundaries, precipitation phases, or dislocation network nodes, and the intermediate portion is pinned by impurity atoms. The dislocation segment length L_N and the average length between the weak pinners L_C are governed by the defects and impurities. The schematic diagram of the changes in the dislocation length with increasing the external stress[30,31] is shown in Fig. 6. When the applied stress is zero, the line (L_N) is pinned by the strong pinners (line A in Fig. 6). With increasing the stress, the loops (L_C) gradually leave the weak pinners and continue to increase until the breakaway stress is reached (evolution from line B to line D in Fig.6). With further increa-

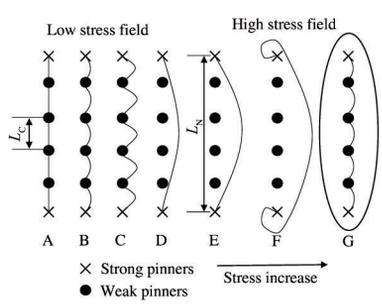

Fig.6 Schematic diagram of G-L dislocation pinning model

sing the stress, the dislocation is also increased (evolution from line E to line F in Fig.6). Then, the new closed dislocation loops form (line G in Fig.6). When the stress is removed, the line (L_N) returns to its original position and is repined.

The $Mg_{94}Zn_5Y_1$ composite has high residual stress around the SiC_p during solidification, which results in a high density of dislocations. It is known from the G-L theory that Q_0^{-1} is proportional to ρ at low strain amplitudes. Hence, in the low-strain-amplitude stage, the damping capabilities of the SiC_p/$Mg_{94}Zn_5Y_1$ composites are better than those of the $Mg_{94}Zn_5Y_1$ alloy.

According to the G-L theory, the relationship of Q_h^{-1} with C_1 and C_2 can be expressed by Eq.(5), as follows:

$$\ln(Q_h^{-1}\varepsilon) = \ln C_1 - C_2/\varepsilon \quad (5)$$

Fig. 7 shows the G-L plots of the composites in the strain amplitude correlation stage, and Table 2 shows the values of C_1 and C_2 of the composites. It can be seen that the C_1 value of the composites with SiC_p addition is greater than that without SiC_p addition, but the C_2 value of the composites with SiC_p addition is smaller than that without the SiC_p addition. According to Eq. (3), the Q_h^{-1} of the composites with SiC_p addition is better than that without the SiC_p addition. According to Eq.(4), the L_C value of the composites with the SiC_p addition is smaller than that without the SiC_p addition. This is mainly because the added SiC_p becomes the heterogeneous nucleation core to promote the formation of quasicrystal phases, which results in a decrease in the solute atoms in the matrix, i. e., the number of weak pinners is decreased. With increasing the SiC_p content, the C_1 value is gradually decreased. It can be seen from Eq. (4) that C_1 is proportional to ρL_N^3. With increasing the content of the reinforcement phase and the secondary phase, the pinning effect of the dislocation becomes more obvious and the dislocation mobility is reduced.

Although various damping mechanisms are functioning in the SiC_p/$Mg_{94}Zn_5Y_1$ composite, the dislocation damping mechanism is in the dominant state. The intrinsic damping mechanism and interface damping mechanism are functioning coordinately. The intrinsic damping mechanism of SiC_p is different from that of the matrix; the intrinsic damping mechanism of the lamellar eutectic phase is also different

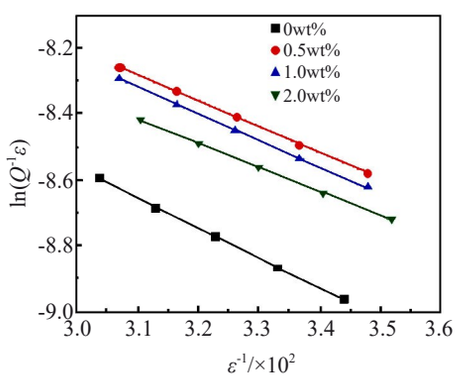

Fig.7 G-L plots of the different SiC_p/$Mg_{94}Zn_5Y_1$ composites

Table 2 Values of C_1 and C_2 of different SiC_p/$Mg_{94}Zn_5Y_1$ composites

SiC_p content/wt%	C_1	C_2/×10²
0	0.0295	0.9125
0.5	0.0457	0.7854
1.0	0.0433	0.8047
2.0	0.0396	0.7377

from that of the primary phase[32]. The structure and properties of different phases in the SiC_p/$Mg_{94}Zn_5Y_1$ composites are different. Therefore, the phase interface and the interface between SiC_p and the matrix both slip under the application of stress and dissipate the energy. The interface between the α-Mg phase and the lamellar eutectic phase also dissipates the energy under the cyclic loading.

2.4 Comprehensive performance

In order to determine the contribution of each parameter to the coordination of the mechanical and damping properties of the composites, the efficiency coefficient method is used to evaluate the comprehensive performance of composite materials. This method is based on the principle of multi-objective planning, which determines the satisfactory value (x_i^h) and unallowable value (x_i^s) for each evaluation index. The satisfactory value is the highest value of the indicator, and the unallowable value is the smallest value of the indicator. The degree of each index (x_i) was calculated to obtain the satisfactory value according to the equation, and the efficiency coefficient of each index can also be obtained. Then the total efficiency coefficient can be calculated according to Eq. (6) and Eq.(7), as follows:

$$f_i = \frac{x_i - x_i^s}{x_i^h - x_i^s} \quad (6)$$

$$F = \frac{\sum_{i=1}^{n} f_i}{n} \quad (7)$$

where the subscript i indicates various indicators; x_i is an index of i indicator; n is the total number of indexes; f_i is the efficiency coefficient of each index; F is the total efficiency coefficient. In the determination of the importance of each evaluation index, the total efficiency coefficient is calculated according to Eq.(7).

In this research, the SiC content in composites has an important influence on the mechanical properties and damping properties of the composites. The comprehensive properties of the SiC_p/$Mg_{94}Zn_5Y_1$ composites are evaluated by the efficiency coefficient method, and the main evaluation indexes are the compressive strength and damping capacities (Q_0^{-1} and Q_h^{-1}), which are equally important.

The efficiency coefficients of the SiC_p/$Mg_{94}Zn_5Y_1$ composites with different SiC_p contents can be calculated according to Eq.(6) and Eq.(7), and the calculation results are shown in Table 3. It can be seen that the efficiency coefficient of the composites with SiC_p addition is much higher than that without SiC_p addition. The comprehensive properties of the

Table 3 Efficiency coefficient *F* of different $SiC_p/Mg_{94}Zn_5Y_1$ composites

SiC_p content/wt%	0	0.5	1.0	2.0
Efficiency coefficient, *F*	0.048	0.581	0.668	0.523

$SiC_p/Mg_{94}Zn_5Y_1$ composites are firstly increased and then decreased with increasing the SiC_p content. The maximum efficiency coefficient is obtained with 1.0wt% SiC_p content, i.e., the optimal synergy between the quasicrystal phase and the SiC_p phases is achieved with 1.0wt% SiC_p content. Hence, the optimal comprehensive properties of the $SiC_p/Mg_{94}Zn_5Y_1$ composites are achieved with 1.0wt% SiC_p content.

3 Conclusions

1) The SiC_p added into the $Mg_{94}Zn_5Y_1$ matrix is distributed evenly in the matrix and refines the composite grains. The $SiC_p/Mg_{94}Zn_5Y_1$ composite is composed of the α-Mg phase, quasicrystal phase, and SiC_p phase.

2) The mechanical properties of the $SiC_p/Mg_{94}Zn_5Y_1$ composites are firstly increased and then decreased with increasing the SiC_p content. The mechanical properties of the composites with SiC_p addition are better than those of the $Mg_{94}Zn_5Y_1$ base alloy. The 1.0wt% $SiC_p/Mg_{94}Zn_5Y_1$ composite has the compressive strength of 350 MPa, which is 12.5% higher than that of the $Mg_{94}Zn_5Y_1$ base alloy.

3) The damping properties of the $SiC_p/Mg_{94}Zn_5Y_1$ composites are slightly improved at the low strain amplitudes. At the strain of 4×10^{-4}, the 0.5wt% $SiC_p/Mg_{94}Zn_5Y_1$ composite shows the highest damping value of 0.011 80, inferring the high-damping material. At high strain, with increasing the SiC_p content, the damping performance is firstly increased and then decreased. The damping properties of all $SiC_p/Mg_{94}Zn_5Y_1$ composites are better than those of the $Mg_{94}Zn_5Y_1$ base alloy, and the best damping capacity is achieved with 0.5wt% SiC_p addition.

4) According to the efficiency coefficient method, the optimal comprehensive properties of the $SiC_p/Mg_{94}Zn_5Y_1$ composites are achieved with 1.0wt% SiC_p addition.

References

1 Liu Enyang, Yu Sirong, Zhao Yan *et al*. *Rare Metal Materials and Engineering*[J], 2017, 46(11): 3298 (in Chinese)

2 Zhai J Y, Song X Y, Xu A Y *et al*. *Metals and Materials International*[J], 2021, 27(6): 1458

3 Ramalingam V V, Ramasamy P, Kovukkal M D *et al*. *Metals and Materials International*[J], 2020, 26(4): 409

4 Agnew S R, Nie J F. *Scripta Materialia*[J], 2010, 63(7): 671

5 Anbuchezhiyan G, Mohan B, Sathyanarayanan D *et al*. *Journal of Alloys and Compounds*[J], 2017, 719: 125

6 Wang X J, Xu D K, Wu R Z *et al*. *Journal of Materials Science & Technology*[J], 2017, 34(2): 245

7 Nie K B, Guo Y C, Deng K K *et al*. *Journal of Alloys and Compounds*[J], 2019, 792: 267

8 Wang Xiaojun, Xiang Yeyang, Hu Xiaoshi *et al*. *Acta Metallurgica Sinica*[J], 2019, 55(1): 73 (in Chinese)

9 Zhang Z Y, Guo Y H, Zhao Y T *et al*. *Materials Characterization* [J], 2019, 150: 229

10 Yu W B, Li X B, Vallet M *et al*. *Mechanics of Materials*[J], 2019, 129: 246

11 Essa Y E S, Fernadez-Saez J, Perez-Castellanos J L. *Journal of Testing and Evaluation*[J], 2003, 31(6): 449

12 Dieringa H. *Fundamentals of Magnesium Alloy Metallurgy*[M]. Cambridge: Woodhead Publishing, 2013: 317

13 Zhen Xu. *Thesis for Master*[D]. Xi'an: Xi'an University of Science and Technology, 2016 (in Chinese)

14 Prasad D S, Shoba C. *Journal of Materials Research and Technology*[J], 2016, 5(2): 123

15 Yan H, Xin H, Hu Q. *Advanced Materials Research*[J], 2010, 123-125: 35

16 Bae D H, Lee M H, Kim K T *et al*. *Journal of Alloys and Compounds*[J], 2002, 342(1-2): 445

17 Yuan G Y, Amiya K, Kato H *et al*. *Journal of Materials Research* [J], 2004, 19(5): 1531

18 Singh A, Tsai A P, Nakamura M *et al*. *Philosophical Magazine Letters*[J], 2003, 83(9): 543

19 Lü Binjiang, Peng Jian, Han Wei *et al*. *Rare Metal Materials and Engineering*[J], 2014, 43(7): 1643 (in Chinese)

20 Singh A, Watanabe M, Kato A *et al*. *Materials Science and Engineering A*[J], 2004, 385(1-2): 382

21 Ma Rong. *Thesis for Master*[D]. Wuhan: Huazhong University of Science and Technology, 2011 (in Chinese)

22 Wan Diqing, Hu Yinglin, Li Zhumin *et al*. *Rare Metal Materials and Engineering*[J], 2019, 48(1): 71

23 Yi S, Park E S, Ok J B *et al*. *Materials Science and Engineering A*[J], 2001, 300(1-2): 312

24 Kim Y K, Kim W T, Kim D H. *Science and Technology of Advanced Materials*[J], 2014, 15(2): 24 801

25 Zhang Y B, Yu S R, Song Y L *et al*. *Journal of Alloys and Compounds*[J], 2008, 464(1-2): 575

26 Long Qiansheng, Wang Weiwei, Ren Guangxiao *et al*. *Foundry Technology*[J], 2016, 37(5): 848 (in Chinese)

27 Huang S J, Ali A N. *Journal of Materials Processing Technology* [J], 2019, 272: 28

28 Ren L B, Zhou M Y, Lu T H *et al*. *Materials Science and Engineering A*[J], 2020, 770: 138 548

29 Wan Diqing, Hu Yinglin, Ye Shuting *et al*. *Journal of Functional Materials*[J], 2018, 49(5): 5035 (in Chinese)

30 Granato A V, Lücke K. *Journal of Applied Physics*[J], 1956, 27(7): 583

31 Granato A V, Lücke K. *Journal of Applied Physics*[J], 1956, 27(7): 789

32 Wan D Q, Wang J C, Wang G F *et al*. *Transactions of Nonferrous Metals Society of China*[J], 2009, 19(1): 45

高阻尼高强度铸态$SiC_p/Mg_{94}Zn_5Y_1$复合材料的综合性能

万迪庆，董少云，王厚彬，胡佳俊，薛雁丹，韩国梁，康　杰，曾观梅，王　玉，汤　浩，杨　帆
(华东交通大学 材料科学与工程学院，江西 南昌 330013)

摘　要：采用铸造方法制备具有不同SiC_p含量（0.5%~2.0%，质量分数，下同）的$SiC_p/Mg_{94}Zn_5Y_1$复合材料，并研究了复合材料的力学性能和阻尼性能。通过扫描电子显微镜和X射线衍射仪测试复合材料的微观组织结构和物相组成。在基体中加入SiC_p之后，SiC_p均匀分布在基体中，增强体细化了复合材料的微观组织结构。$SiC_p/Mg_{94}Zn_5Y_1$复合材料包括α-Mg、I相（准晶相）和SiC_p相。分别使用动态热机械分析仪和AG-X试验机测试了$SiC_p/Mg_{94}Zn_5Y_1$复合材料的阻尼性能和力学性能。复合材料的力学性能优于$Mg_{94}Zn_5Y_1$合金，1.0%$SiC_p/Mg_{94}Zn_5Y_1$复合材料的抗压缩强度高达350 MPa；所有复合材料的阻尼性能都远高于基体合金的阻尼性能，其中0.5%$SiC_p/Mg_{94}Zn_5Y_1$复合材料具有最佳的阻尼性能。此外，根据功效系数法，SiC_p含量为1.0%的$SiC_p/Mg_{94}Zn_5Y_1$复合材料具有良好的综合性能。

关键词：$SiC_p/Mg_{94}Zn_5Y_1$复合材料；准晶；机械性能；阻尼性能

作者简介：万迪庆，男，1981年生，博士，教授，华东交通大学材料科学与工程学院，江西 南昌 330013，电话：0791-87046102，E-mail：divadwan@163.com